Plasma Chem Plasma Process (2017) 37:1445–1462
DOI 10.1007/s11090-017-9820-z

ORIGINAL PAPER

On the Control of Plasma Parameters and Active Species Kinetics in $CF_4 + O_2 + Ar$ Gas Mixture by CF_4/O_2 and O_2/Ar Mixing Ratios

Alexander Efremov[1] · Junmyung Lee[2] · Jihun Kim[2]

Received: 30 January 2017 / Accepted: 28 April 2017 / Published online: 13 May 2017

Abstract The effects of both CF_4/O_2 and Ar/O_2 mixing ratios in three-component $CF_4 + O_2 + Ar$ mixture on plasma parameters, densities and fluxes of active species determining the dry etching kinetics were analyzed. The investigation combined plasma diagnostics by Langmuir probes and zero-dimensional plasma modeling. It was found that the substitution of CF_4 for O_2 at constant fraction of Ar in a feed gas produces the non-monotonic change in F atom density, as it was repeatedly reported for the binary CF_4/O_2 gas mixtures. At the same time, the substitution of Ar for O_2 at constant fraction of CF_4 results in the monotonic increase in F atom density toward more oxygenated plasmas. The natures of these phenomena as well as theirs possible impacts on the etching/polymerization kinetics were discussed in details.

Keywords CF_4-based plasma · Diagnostics · Modeling · Reaction kinetics

Introduction

Fluorocarbon (FC) gases with a general formula of C_xF_y are widely used in the microelectronic industry for dry patterning of silicon wafers and dielectric (SiO_2, Si_3N_4) thin films [1, 2]. Among these, the CF_4 is characterized by the highest F/C ratio and provides the domination of etching over the surface polymerization process under the typical reactive ion etching conditions [3–5]. Being used for the etching process, the CF_4 is frequently combined with Ar or O_2 in forms of binary $CF_4 + Ar$ or $CF_4 + O_2$ gas mixtures

✉ Alexander Efremov
efremov@isuct.ru

[1] Department of Control and Instrumentation Engineering, Korea University, Sejong 30019, South Korea

[2] Department of Electronic Devices and Materials Technology, State University of Chemistry and Technology, 7 Sheremetevsky St., Ivanovo, Russia 153000

with the aims of accelerating the physical etching pathway, increasing the F atoms yield and suppressing polymerization on the surfaces which are in a contact with plasma [4, 5].

Recently, in order to satisfy the increasingly demanding requirements concerning device dimensions and performance, many dry etching processes require optimization through the appropriate choice of working gas and input process conditions. In this framework, an understanding of the plasma chemistry mechanisms involved in various gas systems is important for future progress in the dry etching technology. Until now, there were enough experimental and modeling studies focused on pure CF_4, $CF_4 + Ar$ and $CF_4 + O_2$ low pressure ($p < 50$ mTorr) plasmas [6–16]. These works contain the results of plasma diagnostics by Langmuir probes [6, 7, 10–13], the measurements of the neutral species densities (absorption spectroscopy, optical emission actinometry, mass-spectrometry) [7–9, 13, 16] as well as provide the well-adjusted kinetic schemes determining the steady-state plasma parameters and composition [6, 8, 10, 12–15]. Thought the available data show some disagreements due to different input process conditions and types of plasma reactors, the key features of the $CF_4 + Ar$ and $CF_4 + O_2$ plasma chemistries can briefly be summarized as follows:

- The dilution of CF_4 by Ar at constant pressure and input power has no principal influence on the kinetics of neutral species (except the weak increase in the CF_4 dissociation degree due to an increase in electron density [10–12]), so the densities of F atoms and CF_x radicals decrease monotonically toward Ar-rich plasmas. Another important thing is a growth of positive ion density (due to a decrease in plasma electronegativity that lowers the decay rate of positive ions in ion–ion recombination process) as well as of their flux together with Ar fraction in a feed gas. This accelerates the physical etching pathway for both target material and FC polymer film.
- The dilution of CF_4 by O_2 at constant pressure and input power results in the rapidly decreasing densities of CF_x radicals as well as in the non-monotonic behavior of the F atom density which exhibits a maximum at 20–40% O_2 [13–15]. Most authors reasonably attribute this effect to both stepwise dissociation of the CF_x species due to their interaction with oxygen atoms and the consequent chemical reactions involving the CF_xO products [14, 15].

When analyzing the existing works, one can conclude that modern plasma etching technology involves three- or more component gas mixture, for example $CF_4 + O_2 + Ar$. The ternary gas systems provide more pathways for the changes in gas mixing ratios in order to obtain the optimal process conditions. Particularly, one can fix the fraction of one component and change the mixing ratios for the remaining two ones. It is clear that, since the composition of the feed gas is different compared with the simple $CF_4 + O_2$ mixture, some principal differences in plasma parameters (through the electron energy distribution function and mean electron energy) and densities of plasma active species can take place. Earlier, Kimura and Hanaki [17] have reported the experimental study of $CF_4 + O_2 + Ar$ plasma with variable CF_4 fractions in a feed gas. They found that the behaviors of plasma parameters and F atoms density versus CF_4/O_2 gas mixing ratio at constant Ar fraction are quite similar to those obtained for the $CF_4 + O_2$ plasma. However, they did not provide analysis of plasma chemistry in order to understand the differences between the binary and ternary gas systems. In our previous works have dealt with $CF_4 + O_2 + Ar$ plasma [18, 19], it was found that the variation in Ar/O_2 mixing ratio at constant CF_4 fraction causes the different changes of plasma parameters compared with Ref. [13–15, 17] as well as does not result in the non-monotonic behavior of F atoms density. Unfortunately, the data of Refs. [17–19] cannot be compared directly and/or analyzed in a comparative scale

because of different input process conditions, reactor types and geometries. Another important thing is that all mentioned studies were mainly focused on bulk plasma characteristics and thus, did not provide enough information on the possible impacts of CF_4/O_2 and Ar/O_2 mixing ratios on the dry etching kinetics. Such situation retards the optimization of the dry etching technologies with using the $CF_4 + O_2 + Ar$ plasma.

The goal of this work was the study of $CF_4 + O_2 + Ar$ inductively coupled plasma under the fixed set of operating conditions (gas pressure, input power and bias power), but in two different gas mixing regimes assumed the change in CF_4/O_2 or Ar/O_2 mixing ratio. In other words, we would like to demonstrate the ability of $CF_4 + O_2 + Ar$ gas system to adjust the plasma parameters and composition using the gas mixing ratios only. For this purpose, we applied the previously used research scheme based on plasma diagnostics by Langmuir probes and 0-dimensional plasma modeling [18]. The main attention was focused on the comparative analysis of the parameters which directly determine the dry etching mechanisms: ion energy flux, F atom flux, ion energy flux, F atom flux, polymerizing species (CF_2 and CF) flux as well as various flux-to-flux ratios illustrating the changes in the etching/polymerization balance. We also performed the analysis of the formation-decay kinetics for neutral species in order to explain the obtained phenomena.

Experimental and Modeling Details

Experimental Setup and Plasma Diagnostics

The experiments were performed in planar inductively coupled plasma (ICP) reactor [20]. The reactor had a cylindrical ($r = 15$ cm) chamber made from the anodized aluminum. The 5-turns copper coil with a diameter of 29 cm was connected to the 13.56 MHz power supply and located above the 10 mm thick-horizontal quartz window on the top side of the chamber. A distance (l) between the window and the bottom electrode used as a substrate holder was 12.8 cm. The bottom electrode was connected to 12.56 MHz power supply to maintain a negative dc bias voltage ($-U_{dc}$). The temperature of the bottom electrode was stabilized at 17 °C using the water-flow cooling system.

All experimental series corresponded to the fixed total gas flow rate ($q = 40$ sccm), gas pressure ($p = 6$ mTorr) and input power ($W = 900$ W). The input power density $W' = W/\pi r^2 l$ then became 0.9 W cm^{-3}. In order to imitate actual etching conditions, the bottom electrode was biased by $W_{dc} = 200$ W. The initial $CF_4 + O_2 + Ar$ gas compositions were set by adjusting the partial flow rates. In one experimental series, the CF_4 flow rate was fixed at 20 sccm while the flow rates of the O_2 and Ar were variably set to a combined total of $q_{O_2} + q_{Ar} = 20$ sccm. Therefore the fraction of CF_4 ($y_{CF_4} = q_{CF_4}/q$) in the feed gas was always 0.5, and the remaining half gas mixture was composed of various amounts of Ar and O_2. Another experimental series assumed the constant flow rate for Ar ($q_{Ar} = 20$ - sccm) as well as the variable flow rates for CF_4 and O_2, so that $q_{O_2} + q_{CF_4} = 20$ sccm. In this case, the fraction of Ar ($y_{Ar} = q_{Ar}/q$) in the feed gas was always 0.5, and the remaining half gas mixture was composed of various amounts of CF_4 and O_2.

The plasma parameters were determined by a double Langmuir probe (LP), (DLP2000, Plasmart Inc.). The probe tip was installed through a hole in the sidewall of the chamber, 5.7 cm above the bottom electrode and centered in a radial direction. The output data were the electron temperature (T_e), ion current density (J_+), floating potential (U_f), and total positive ion density (n_+). The treatment of the I–V curves was based on Johnson and

Malter's double probe theory [21] and the Allen–Boyd–Reynolds (ABR) approximation for the ion saturation current density [22]. These assume $J_+ \approx 0.61\, en_+ \upsilon$, where υ is the ion Bohm velocity. In our previous studies, it was shown that such an approach can be reasonably applied even for more electronegative plasmas than those used in this study [23, 24]. The effective ion mass needed to determine υ was evaluated simply through the mole fractions of the corresponding neutral species. In order to exclude the influence of the FC polymer film on the LP results, we conducted a set of preliminary experiments, where the $I-V$ curves were recorded continuously at fixed-feed gas composition and operating parameters. Even for the non-oxygenated 50% CF_4 + 50% Ar plasma, the differences between the results of such measurements did not exceed the standard experimental error for a period of at least 10 min after the plasma was turned on. Also, throughout the main experimental procedure, the probe tip was cleaned in 50% Ar + 50% O_2 plasma before and after each measurement.

Plasma Modeling

In order to obtain the densities and fluxes of plasma active species, we used a simplified zero-dimensional kinetic model with the experimental data on T_e and n_+ as input parameters [23, 24]. Similarly to our previous works [18, 19], the model was based on the well-adjusted reaction scheme (see Table 1) and used the following assumptions:

1. The electron energy distribution function (EEDF) is quite close to Maxwellian one. The applicability of Maxwellian EEDFs for the description of the electron-impact kinetics for CF_4-based low-pressure ($p < 50$ mTorr) ICPs has been confirmed in many works by reasonable agreements between the measured and model-predicted plasma parameters [12–14]. Also, Kimura et al. [13] reported that the experimentally determined EEDFs in CF_4 plasma at $p < 20$ mTorr had the almost Maxwellian shapes. The postulation of Maxwellian EEDF allows one to obtain the rate coefficients for the electron-impact processes (R1–R17) as functions of T_e in a form of $k = AT_e^B \exp(-C/T_e)$ [13, 14].
2. The half-diluted CF_4 gas does not form a continuous FC polymer film on the chamber walls under plasma conditions [4, 25]. This allows one to describe the heterogeneous chemistry of atoms (F, C, O) and radicals (CF_3, CF_2, CF) in terms of the conventional first-order recombination kinetics. The rate coefficients for the heterogeneous loss of these species (R51–R56) can be evaluated as $k_S \approx \gamma \upsilon_T / \Lambda$, where $\Lambda = \left[(2.405/r)^2 + (\pi/l)^2\right]^{-1/2}$ is the diffusion length [5], $\upsilon_T = (8k_B T_{gas}/\pi m)^{1/2}$, and γ is the recombination probability. The recombination probabilities for F ($\gamma_F \approx 0.02$), CF_3 ($\gamma_{CF_3} \approx 0.05$), CF_2 ($\gamma_{CF_2} \approx 0.1$) and CF ($\gamma_{CF} \approx 0.1$) species were taken from the modeling works [12, 13, 26] where these were adjusted in order to obtain the agreement between the measured and model-predicted densities of F atoms and CF_2 radicals in CF_4- and C_4F_8-based plasmas. All reaction pathways between the adsorbed (marked by the "s" index) and gaseous species inside R51–R56 were assumed to have equal probabilities of occurrence.
3. The temperature of the neutral ground-state species (gas temperature, T_{gas}) is independent of the feed gas composition [18, 19]. Since experimental data on T_{gas} were not available during this study, we took 600 K as the typical value for close ranges of p and W' in ICP etching reactors with similar geometry [18, 19, 23, 24].

Table 1 Reduced reaction set for the modeling of neutral species chemistry in $CF_4 + O_2 + Ar$ plasma

Process		Rate coefficient ($cm^3\ s^{-1}$)			
		ε_{th} (eV)	A	B	C
R1	$CF_4 + e = CF_3 + F + e$	5.60	1.38×10^{-8}	0	16
R2	$CF_4 + e = CF_2 + 2F + e$	9.50	2.22×10^{-10}	0.99	14.77
R3	$CF_4 + e = CF_3^+ + F + 2e$	15.9	9.36×10^{-8}	0	20.4
R4	$CF_4 + e = CF_3 + F^+ + 2e$	23.10	9.79×10^{-10}	0.94	34.67
R5	$CF_3 + e = CF_2 + F + e$	3.80	6.48×10^{-8}	−0.959	11.25
R6	$CF_2 + e = CF + F + e$	5.40	8.11×10^{-9}	0.386	8.739
R7	$CF_2 + e = C + 2F + e$	11.00	1.39×10^{-8}	−1.164	49.87
R8	$CF + e = C + F + e$	5.60	1.63×10^{-8}	−0.002	13.05
R9	$F_2 + e = 2F + e$	4.34	1.08×10^{-8}	−0.296	4.464
R10	$O_2 + e = 2O + e$	6.40	1.52×10^{-9}	0	4.15
R11	$O_2 + e = O + O(^1D) + e$	8.57	2.04×10^{-8}	0	8.18
R12	$CO_2 + e = CO + O + e$	13.50	1.87×10^{-8}	0	13.89
R13	$CO + e = C + O + e$	13.50	1.87×10^{-8}	0	13.89
R14	$O + e = O(^1D) + e$	1.97	4.47×10^{-9}	0	2.29
R15	$FO + e = F + O + e$	4.30	6.16×10^{-9}	0	4.30
R16	$CFO + e = CO + F + e$	5.40	8.11×10^{-9}	0.386	8.739
R17	$CF_2O + e = CFO + F + e$	3.80	6.48×10^{-8}	−0.959	11.25
R18	$F_2 + CF_3 = CF_4 + F$	6.31×10^{-14}			
R19	$F_2 + CF_2 = CF_3 + F$	7.94×10^{-14}			
R20	$F_2 + CF = CF_2 + F$	3.98×10^{-12}			
R21	$F_2 + O = FO + F$	1.00×10^{-16}			
R22	$F_2 + O(^1D) = FO + F$	7.94×10^{-12}			
R23	$F_2 + CFO = CF_2O + F$	5.01×10^{-14}			

Table 1 continued

Process		Rate coefficient ($cm^3\ s^{-1}$)			
		ε_{th} (eV)	A	B	C
R24	$CF_3 + F = CF_4$	1.00×10^{-12}			
R25	$CF_3 + O = CF_2O + F$	3.16×10^{-11}			
R26	$CF_3 + O(^1D) = CF_2O + F$	3.16×10^{-11}			
R27	$CF_2 + F = CF_3$	4.17×10^{-13}			
R28	$CF_2 + O = CFO + F$	3.16×10^{-11}			
R29	$CF_2 + O(^1D) = CFO + F$	3.16×10^{-11}			
R30	$CF_2 + O = CO + 2F$	3.98×10^{-12}			
R31	$CF_2 + O(^1D) = CO + 2F$	3.98×10^{-12}			
R32	$CF + F = CF_2$	5.01×10^{-15}			
R33	$CF + O = CO + F$	6.31×10^{-11}			
R34	$CF + O(^1D) = CO + F$	2.00×10^{-11}			
R35	$CF + O_2 = CFO + O$	3.16×10^{-11}			
R36	$FO + O = F + O_2$	2.51×10^{-11}			
R37	$FO + O(^1D) = F + O_2$	5.01×10^{-11}			
R38	$FO + FO = 2F + O_2$	2.51×10^{-12}			
R39	$2FO = F_2 + O_2$	2.51×10^{-16}			
R40	$CFO + CF_3 = CF_4 + CO$	1.00×10^{-11}			
R41	$CFO + CF_3 = CF_2O + CF_2$	1.00×10^{-11}			
R42	$CFO + CF_2 = CF_3 + CO$	3.16×10^{-13}			
R43	$CFO + CF_2 = CF_2O + CF$	3.16×10^{-13}			
R44	$CFO + O = CO_2 + F$	1.00×10^{-10}			
R45	$CFO + O(^1D) = CO_2 + F$	1.00×10^{-10}			
R46	$2CFO = CF_2O + CO$	1.00×10^{-11}			

Table 1 continued

Process		Rate coefficient ($cm^3\ s^{-1}$)			
		ε_{th} (eV)	A	B	C
R47	$CFO + F = CF_2O$	7.94×10^{-11}			
R48	$CF_2O + O(^1D) = F_2 + CO_2$	2.00×10^{-11}			
R49	$C + O_2 = CO + O$	1.58×10^{-11}			
R50	$CO + F = CFO$	1.29×10^{-11}			
R51	$F = F(s) + CF_3 = CF_4 + CF_2 = CF_3 + CF = CF_2 + F = F_2 + C = CF + O = FO$	$f(\gamma)$, $\gamma = 0.02$			
R52	$CF_3 = CF_3(s) + F = CF_4$	$f(\gamma)$, $\gamma = 0.05$			
R53	$CF_2 = CF_2(s) + F = CF_3 + O = CF_2O$	$f(\gamma)$, $\gamma = 0.1$			
R54	$CF = CF(s) + F = CF_2 + O = CFO$	$f(\gamma)$, $\gamma = 0.1$			
R55	$C = C(s) + F = CF + O = CO$	$f(\gamma)$, $\gamma = 1$			
R56	$O = O(s) + O = O_2 + F = FO + C = CO + CF = CFO + CF_2 = CF_2O$	$f(\gamma)$, $\gamma = 0.1$			
R57	$O(^1D) = O$	$f(\gamma)$, $\gamma = 1$			
R58	$CF_3^+ = CF_3$	υ/d_c, where $\upsilon \approx \sqrt{eT_e/m_i}$ and $d_c = 0.5rl/(rh_l + lh_r)$			
R59	$F^+ = F$				

Accordingly, the rate coefficients for R18–R50 were taken from the NIST chemical kinetics database [27] for $T_{gas} = 600$ K.

4. For the given range of operating parameters, the formation of C_xF_y species with $x > 1$ may be neglected due to their low densities and negligible influence on the overall reaction balance [23].

The steady-state electron density (n_e) was calculated using the simultaneous solution of the chemical kinetic equation for negative ions and the quasi-neutrality condition $n_+ = n_e + n_-$. When neglecting the loss of negative ions on reactor walls [5], their kinetic equation for the given gas system may be written as

$$\left(k_{da,CF_4} n_{CF_4} + k_{da,F_2} n_{F_2} + k_{da,O_2} n_{O_2}\right) n_e \approx k_{ii} n_+ n_- \tag{1}$$

where k_{da} is the dissociative attachment rate coefficients for corresponding species, n_- is the density of negative ions, and $k_{ii} \approx 1 \times 10^{-7}$ cm^3 s^{-1} is the rate coefficient for ion–ion recombination. Accordingly, the left-hand side of Eq. (1) represents the total formation rate for negative ions while the right-hand side is their total decay rate in bulk plasma. These allow one to obtain

$$n_e \approx \frac{k_{ii} n_+^2}{\nu_{da} + k_{ii} n_+} \tag{2}$$

where $\nu_{da} \approx k_{da,CF_4} n_{CF_4} + k_{da,F_2} n_{F_2} + k_{da,O_2} n_{O_2}$ is the total frequency of dissociative attachment. The rate coefficients k_{da} were taken from Refs. [13, 14].

The steady-state densities for neutral species were obtained from the system of chemical kinetics equations in the general form of $R_F - R_D = (k_s + 1/\tau_R)n$, where R_F and R_D are the volume-averaged formation and decay rates in bulk plasma for a given type of species, n is their density, $\tau_R = (1/p_0)\pi r^2 lp/q$ is the residence time and $p_0 = 101{,}325$ Pa is the gas pressure corresponding to standard conditions. The fluxes of F atoms (Γ_F), O atoms (Γ_O) and polymerizing radicals ($\Gamma_{pol} = \Gamma_{CF} + \Gamma_{CF_2}$) to the etched surface were calculated in one and the same manner as $\Gamma \approx 0.25 n \sqrt{8 k_B T_{gas}/\pi m}$. The total flux of positive ions was simply evaluated as $\Gamma_+ \approx J_+/e$. The applicability of both modeling algorithm and reaction schemes for the given range of process conditions have been confirmed in our previous works [18, 19] by the decent agreement between model-predicted and measured densities for F atoms and CF_2 radicals.

Results and Discussion

When the fluorocarbon-based plasmas are used for the etching process, the changes of the etching rate versus operating parameters depend on two main factors, and namely on (1) the fluxes of plasma active species (chemically active neutrals, energetic ions) and (2) the steady-state structure and thickness of the deposited FC polymer film [4, 5]. According to Refs. [28, 29], the growth of the FC polymer on the etched surface is mainly provided by the fluorocarbon radicals with more than one free bonds while both oxygen atoms and positive ions etch the FC polymer film by chemical and physical pathways, respectively. Therefore, the species of principal interest which determine the dry etching mechanisms in $CF_4 + O_2 + Ar$ plasma are F atoms, O atoms, CF_x ($x = 1, 2$) radicals and positive ions.

Figures 1 and 2 represent measured and model-predicted plasma parameters and densities of charged species as functions of CF_4/O_2 and Ar/O_2 gas mixing ratios in

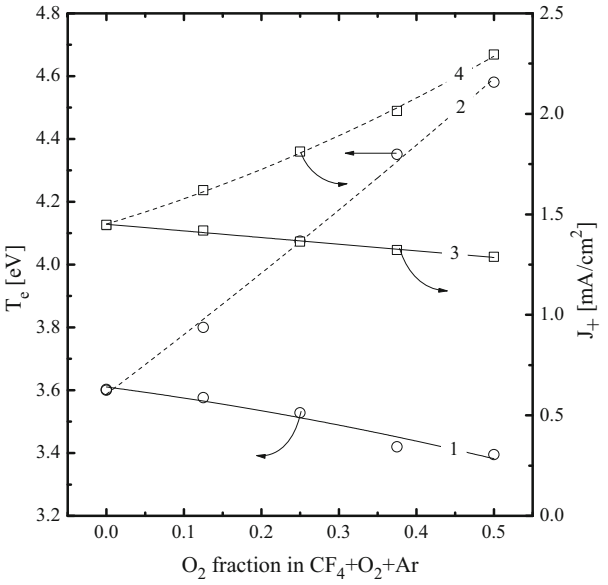

Fig. 1 Measured electron temperature (*1*, *2*) and ion current density (*3*, *4*) in $CF_4 + O_2 + Ar$ plasma as functions of both O_2/Ar mixing ratio at $y_{CF_4} = \text{const}$ (*1*, *3*) and CF_4/O_2 mixing ratio at $y_{Ar} = \text{const}$ (*2*, *4*). The input process conditions are: $p = 6$ mTorr, $W_{inp} = 900$ W and $W_{dc} = 200$ W

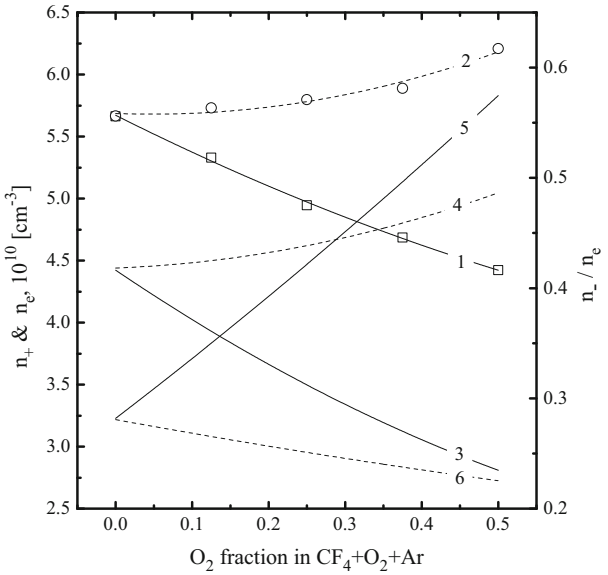

Fig. 2 Measured positive ion density (*1*, *2*) as well as model-predicted electron density (*3*, *4*) and relative density of negative ions (*5*, *6*) in $CF_4 + O_2 + Ar$ plasma as functions of both O_2/Ar mixing ratio at $y_{CF_4} = \text{const}$ (*1*, *3* and *5*) and CF_4/O_2 mixing ratio at $y_{Ar} = \text{const}$ (*2*, *4* and *6*). The input process conditions correspond to Fig. 1

$CF_4 + O_2 + Ar$ gas mixture. From Fig. 1, it can be seen that the substitution of Ar for O_2 at $y_{CF_4} = \text{const}$ results in decreasing both T_e (3.6–3.4 eV for 0–50% O_2) and J_+ (1.5–1.3 mA cm^{-2} for 0–50% O_2) that corresponds to $n_+ = 5.7 \times 10^{10}$–4.4×10^{10} cm^{-3}. Oppositely, the substitution of CF_4 for O_2 at $y_{Ar} = \text{const}$ causes an increase in electron temperature ($T_e = 3.6$–4.6 eV for 0–50% O_2) and ion current density ($J_+ = 1.5$–2.3 mA cm^{-2} for 0–50% O_2). Accordingly, an increase in J_+ provides the same behavior of total positive ion density ($n_+ = 5.7 \times 10^{10}$–6.2×10^{10} cm^{-3} for 0–50% O_2). In both

cases, the model-predicted electron density follows the behavior n_+ and changes as 4.4×10^{10}–2.8×10^{10} cm^{-3} for 0–50% O_2 at $y_{CF_4} = \text{const}$ and 4.4×10^{10}–5.1×10^{10} cm^{-3} for 0–50% O_2 at $y_{Ar} = \text{const}$ (Fig. 2). From Fig. 2, it can be seen also that the total density of negative ions in the case of $y_{CF_4} = \text{const}$ monotonically increases in the range of 1.3×10^{10}–1.6×10^{10} cm^{-3} for 0–50% O_2 that provides $n_-/n_e = 0.28$–0.58. At the same time, the change in CF_4/O_2 mixing ratio at $y_{Ar} = \text{const}$ slightly lowers both n_- (1.3×10^{10}–1.1×10^{10} cm^{-3} for 0–50% O_2) and n_-/n_e (0.28–0.23 for 0–50% O_2). The analysis of these data allows one to explain the differences in plasma parameters influencing the kinetics of electron impact reactions in given gas systems as follows:

- The behavior of T_e is determined by the changes in the electron energy losses in inelastic collisions with plasma species. The substitution of Ar by O_2 at $y_{CF_4} = \text{const}$ increases the overall electron energy loss because the molecular gas has more excitation pathways than the noble one. Really, the first excitation potential for Ar atoms is ~11.6 eV while the O_2 molecules provide the continuous election energy loss starting from ~0.2 eV [5, 6, 13]. The last feature is provided by the vibrational excitation of ground-state O_2 ($\varepsilon_{th} = 0.16$ eV, where ε_{th} is the threshold energy) as well by the formation of metastable electronically excited states $O_2(a^1\Delta)$ with $\varepsilon_{th} = 0.98$ eV and $O_2(b^1\Sigma)$ with $\varepsilon_{th} = 1.64$ eV [30]. Oppositely, an increase in O_2 fraction at $y_{Ar} = \text{const}$ decreases the overall electron energy loss for vibrational and low-threshold electronic excitations. The reason is that the corresponding cross-sections (and thus, the partial electron energy losses determined by the parameter $\varepsilon_{th}k$, where k is the process rate coefficient) for CF_4-related species are higher compared with those for O_2 molecules [30, 31].
- The behavior of n_e (and thus, of n_+ and n_- with accounting for the quasi-neutrality condition) is determined by the change in the formation-decay balance for charged species. Particularly, Fig. 3 shows the influence of CF_4/O_2 and Ar/O_2 mixing ratios on the ionization frequencies for dominant neutral species (ν_{iz}) determines as the multiplications of their densities and corresponding ionization rate coefficients (k_{iz}) [12, 13, 17]. In the non-oxygenated 50% CF_4 + 50% Ar plasma, the main contribution to the total ionization rate belongs to ground-state Ar atoms. Such situation appears due to $k_{iz,Ar} > k_{iz,CF_4}$ ($\sim 6.9 \times 10^{-10}$ cm^3 s^{-1} and $\sim 3.3 \times 10^{-10}$ cm^3 s^{-1}, respectively, at $T_e = 3.6$ eV). Since the values of k_{iz} are highly sensitive to electron temperature (due to $\varepsilon_{iz} \approx$ 12–15 eV $> (3/2)T_e$, where ε_{iz} is the threshold energy for ionization [5, 16], and $(3/2)T_e$ is the mean electron energy), the change in T_e (and thus, in gas mixing ratios) noticeably influences the ionization efficiency in both gas systems. The substitution of Ar for O_2 at $y_{CF_4} = \text{const}$ lowers both $k_{iz,Ar}$ and n_{Ar} while a decrease in $\nu_{iz,Ar}$ is not compensated by the impacts from the oxygen-containing species (Fig. 3a). Therefore, the change in Ar/O_2 mixing ratio toward more oxygenated plasmas suppresses the ionization (total $\nu_{iz} = 4.3 \times 10^4$–$2.0 \times 10^4$ s^{-1}, and $\nu_{iz}n_e = 1.9 \times 10^{15}$–$5.6 \times 10^{14}$ cm^{-3} s^{-1} for 0–50% O_2) and thus, lowers the formation rates for both electrons and positive ions. Simultaneously, the substitution of the electropositive component for the electronegative one increases the formation rate for negative ions, lifts up plasma electronegativity as well as accelerates decay of positive ions and electrons in bulk plasma. In the case of $y_{Ar} = \text{const}$, one can obtain an opposite situation. An increasing O_2 fraction in a feed gas lifts up the total ionization frequency through both increasing $\nu_{iz,Ar}$ ($k_{iz,Ar} = 6.9 \times 10^{-10}$–$2.2 \times 10^{-9}$ cm^3 s^{-1} for 0–50% O_2) and the noticeable contribution from ν_{iz,O_2} at $y_{O_2} > 40\%$ (Fig. 3b). The last

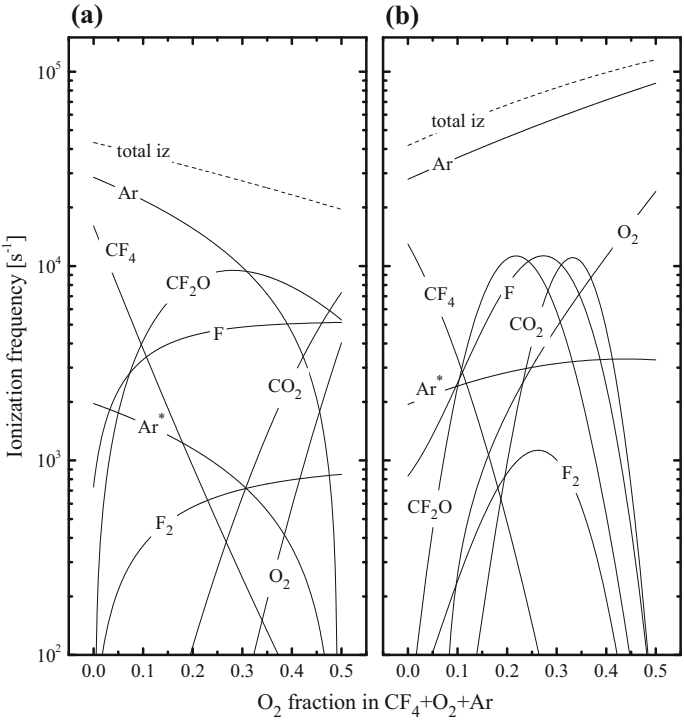

Fig. 3 Ionization frequencies for dominant neutral species in $CF_4 + O_2 + Ar$ plasma at $y_{CF_4} = \text{const}$ (**a**) and $y_{Ar} = \text{const}$ (**b**). The term "total iz" means the total ionization frequency

effect is provided by the condition $k_{iz,O_2} > k_{iz,CF_4}$ due to the corresponding differences in their ionization cross-sections [31, 32]. As a result, one can obtain a monotonic increase in both total ionization frequency (4.3×10^4–1.1×10^5 s^{-1} for 0–50% O_2) and ionization rate (1.9×10^{15}–5.7×10^{15} cm^{-3} s^{-1} for 0–50% O_2). Simultaneously, the lower electronegativity of O_2 ($k_{da,O_2} = 2.3 \times 10^{-11}$–$3.4 \times 10^{-11}$ cm^3 s^{-1} for 0–50% O_2) compared with CF_4 ($k_{da,CF_4} = 3.9 \times 10^{-11}$–$4.2 \times 10^{-11}$ cm^3 s^{-1} for 0–50% O_2) provides the weak monotonic decrease in both formation rate and density of negative ions. This slightly reduces the decay rates of both electrons and positive ions through dissociative attachment and ion–ion recombination, respectively.

Figures 4 and 5 illustrate kinetics and densities in neutral species in $CF_4 + O_2 + Ar$ plasmas with various CF_4/O_2 and Ar/O_2 gas mixing ratios. As can be seen from Fig. 4, in the non-oxygenated 50% CF_4 + 50% Ar plasma, the main source of F atoms are the electron-impact dissociations of CF_4 (R1, R3) and CF_3 (R5). These processes constitute approximately 85% of the total F atom formation rate while the contribution from the CF_2 and CF radicals through R6 and R8 does not exceed 5%. The remaining 10% comes from R9, which is supported by the high $F \rightarrow F_2$ recombination rate on the reactor walls in R51. Accordingly, the decay of F atoms is mainly caused by their heterogeneous recombination in R51–R55 while the rate of the fastest bulk process R24 is about 10 times less.

The substitution of Ar for O_2 at $y_{CF_4} = \text{const}$ noticeably reduces the rates of R1, R3 and R5 even in the low-oxygenated ($y_{O_2} < y_{Ar}$) gas mixtures (Fig. 4a) due to the simultaneous decrease in n_e, n_{CF_4} (3.5×10^{13}–1.9×10^{13} cm^{-3} for 0–12% O_2), and n_{CF_3} (5.2×10^{12}–

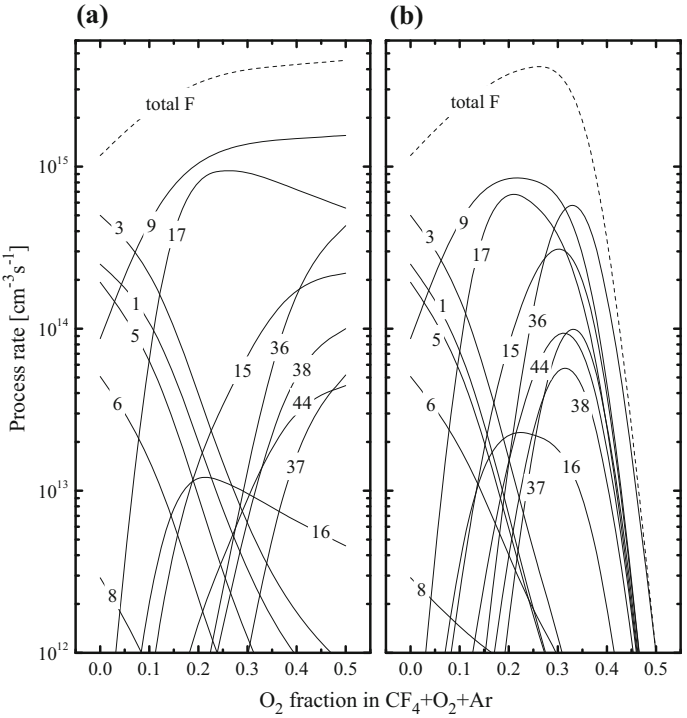

Fig. 4 Fluorine atom formation kinetics in $CF_4 + O_2 + Ar$ plasma at $y_{CF_4} = \text{const}$ (**a**) and $y_{Ar} = \text{const}$ (**b**). The labels on the curves correspond to reaction numbers in Table 1. The term "total F" means the total formation rate for fluorine atoms

1.9×10^{12} cm^{-3} for 0–12% O_2) (Fig. 5a). The density of CF_3 radicals decreases because of their decomposition in R25, R26, R40 and R41 with the participation of O, O(^{1}D), and CFO. The behavior of n_{CF_4} follows that of n_{CF_3} because the latter represent the main source of CF_4 molecules in the plasma chemical reactions. At the same time, the addition of O_2 introduces new channels for the formation of F atoms involving CFO (R16) and CF_2O (R17), while also accelerating R9. The high formation rate for the CFO species is provided by R17 and R50, while CF_2O is effectively formed in R41, R46 and R47. The acceleration of R9 is due to the rapidly increasing F_2 density ($n_{F_2} = 9.2 \times 10^{11}$–$9.0 \times 10^{12}$ cm^{-3} for 0–12% O_2) because of the formation of these species in R48 and heterogeneous recombination of F atoms. As a result, the total F atom formation rate increases compared with the 50% CF_4 + 50% Ar plasma, which causes an increase in F atom density ($n_F = 5.8 \times 10^{12}$–2.6×10^{13} cm^{-3} for 0–12% O_2). The transition to the high-oxygenated ($y_{O_2} > y_{Ar}$) gas mixtures maintains all the previously mentioned tendencies for reaction rates while also introducing additional mechanisms for the formation of F atoms. Particularly, the electron impact dissociation rate of the FO species (R15) reaches the levels of R16 and R17, and the total effect of R15–R17 becomes greater than the sum of R1, R3 and R5. The high formation rate and density of FO molecules (8.2×10^{10}–6.3×10^{12} cm^{-3} for 12–50% O_2) are provided mainly by R22 and the heterogeneous interaction between F and O atoms in R51 and R56. Additionally, the rates of the atom-molecular processes R22, R36–R38 and R44 increase together with the increasing O_2 content in the feed gas and,

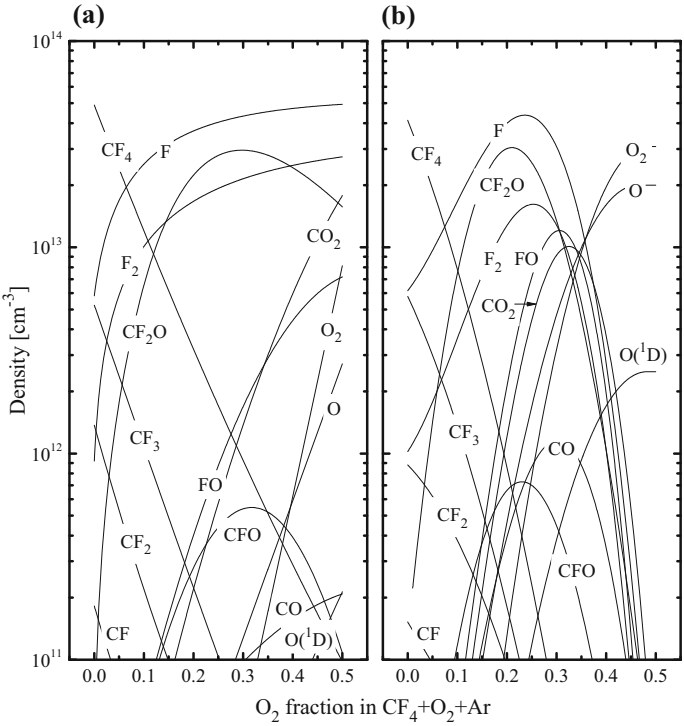

Fig. 5 Model-predicted densities of neutral species in $CF_4 + O_2 + Ar$ plasma at $y_{CF_4} = \text{const}$ (**a**) and $y_{Ar} = \text{const}$ (**b**)

finally, appear to be comparable with R15–R17. Therefore, the substitution of Ar for O_2 at $y_{CF_4} = \text{const}$ provides a continuous increase in the F atom formation rate (Fig. 4a) and thus, the F atom density (Fig. 5a).

The substitution of CF_4 for O_2 at $y_{Ar} = \text{const}$ is escorted by the decreasing amount of CF_4 in a feed gas and thus, results in much faster decrease in the rates of R1, R3 and R5 (Fig. 4b) as well as in deeper falls in the densities of fluorocarbon radicals (Fig. 5b). However, until the condition $y_{O_2} < y_{CF_4}$ is valid, the kinetics of F atoms is quite similar to the described above. Here, and increase in F atom formation rate and density is provided by the rapidly increasing rates of R15–R17 and R36 with a participation of FO, CFO and CF_2O. At one and the same y_{O_2}, the densities of these species appears to be noticeably higher than in previous case because of the higher densities of both O and O(^{1}D). The last effect is connected with the higher formation rate for oxygen atoms in R10, R11 and R14 due to increasing n_e as well as with their lower consumption in R25, R26, R28 and R29. At the same time, the transition to the high-oxygenated ($y_{O_2} > y_{CF_4}$) gas mixtures changes the situation due to the lack of fluorine-containing species. Particularly, the deep decrease in n_{CF}, n_{CF_2} and n_{CF_3} limits the formation of CFO and CF_2O species through both volume (R40, R41, R50) and heterogeneous (R53, R54, R56) processes. That is why the rates of R15–R17 and R44 exhibit a maximum at about 25–30% O_2. Simultaneously, an increasing consumption of F_2 in R22 limits the formation of F atoms through R9 which also losses an increasing tendency after 25% O_2. Since R22 represents the sufficient source of FO, the maximums on the density of these species as well as on the rates of R36–R38 are shifted

toward more oxygenated plasmas and appear at about 35% O_2. All these result in the non-monotonic changes in both total F atom formation rate (Fig. 4b) and F atom density (Fig. 5b). In fact, the difference between $CF_4 + O_2 + Ar$ with $y_{Ar} = \text{const}$ and binary $CF_4 + O_2$ plasmas under one and the same operating conditions is only in the absolute values of species densities due to the different values of T_e and n_e in the presence of Ar. From Fig. 5, it can be understood also that the highest values of F atom density, n_F^{max}, in the gas systems with $y_{CF_4} = \text{const}$ and $y_{Ar} = \text{const}$ are different and obtained at different fractions of O_2 in a feed gas. Particularly, when the substitution of Ar for O_2 at $y_{CF_4} = \text{const}$ takes place, $n_F^{max} = 4.9 \times 10^{13}$ cm^{-3} at 50% O_2. At the same time, the substitution of CF_4 for O_2 at $y_{Ar} = \text{const}$ results in $n_F^{max} = 3.1 \times 10^{13}$ cm^{-3} at 25% O_2. The remarkable thing is that, in both cases, n_F^{max} corresponds to $y_{O_2} \approx y_{CF_4}$. This is because the near-to-equal amounts of CF_4 and O_2 in a feed gas provide the best conditions for both homogeneous and heterogeneous reactions between their dissociation products.

Since the most of dry etching processes in fluorocarbon-based plasmas are provided by the ion-assisted chemical reaction [3–5], the issue of key interest is to compare how the changes in CF_4/O_2 and Ar/O_2 mixing ratios influence physical and chemical etching pathways. In the case if the chemical etching pathway is driven by F atoms, the rate of heterogeneous chemical reaction may be taken as $\gamma_R \Gamma_F$ [33–35], where Γ_F is the flux of fluorine atoms, and γ_R is the reaction probability. Then, assuming $\gamma_R \approx \text{const}$ at constant

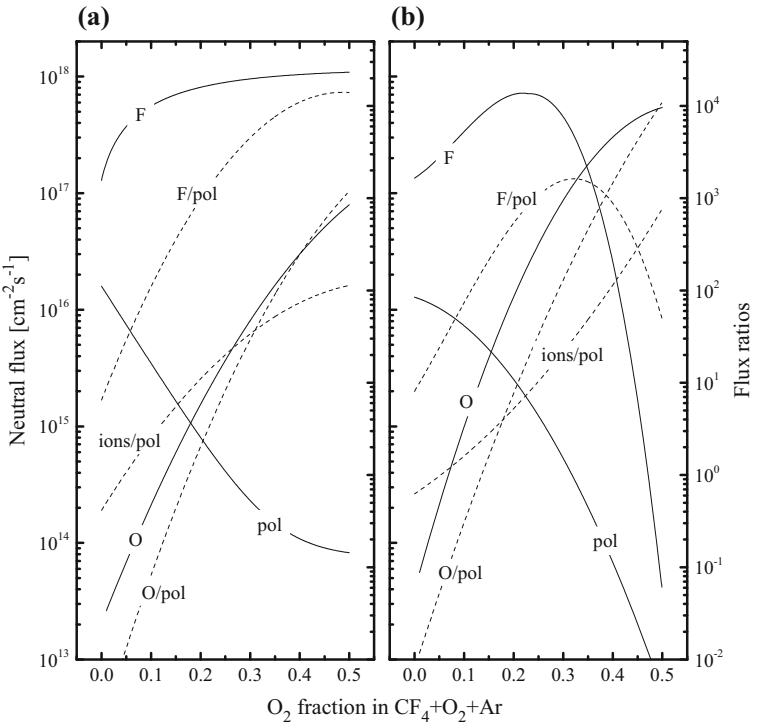

Fig. 6 Model-predicted fluxes (*solid lines*) and flux-to-flux ratios (*dashed lines*) in $CF_4 + O_2 + Ar$ plasma: **a** as functions of O_2/Ar mixing ratio at $y_{CF_4} = \text{const}$; **b** as functions of CF_4/O_2 mixing ratio at $y_{Ar} = \text{const}$. The label "ions" means the total positive ion flux while the label "pol" relates to the flux of polymerizing radicals

surface temperature, the changes in the chemical etching pathway with variations of CF_4/O_2 and Ar/O_2 mixing ratios may be characterized by the changes in Γ_F only. The data of Fig. 6 indicate that the fluxes of F atoms follow the behaviors of theirs densities and show the same differences with increasing fraction of O_2 in a feed gas. Accordingly, taking in mind the points corresponding to n_F^{max}, one can say that the $CF_4 + O_2 + Ar$ plasma with $y_{CF_4} = \text{const}$ provides by $\sim 60\%$ higher efficiency of the chemical etching pathway for one and the same etched material. The role of ion bombardment in the $CF_4 + O_2 + Ar$ plasma may include the sputtering of the native surface atoms, the ion-stimulated desorption of low-volatility reaction products, and the destruction of the FC polymer film. From published works [27, 33–36], it can be understood that the rate of any mentioned physical etching pathway is given by $Y_S\Gamma_+$, where Y_S is the ion-type-averaged sputtering yield. For the ion bombardment energy $\varepsilon_i < 500$ eV, one can assume Y_S to be proportional to the energy transferred by the incident ion to the surface atom [28]. Therefore, the efficiency of the physical etching pathway can be characterized by the ion energy flux $\varepsilon_i\Gamma_+$, where $\varepsilon_i \approx e|-U_f-U_{dc}|$, and U_f is the floating potential. The data of Fig. 7 shows that the substitution of Ar for O_2 at $y_{CF_4} = \text{const}$ results in increasing $-U_{dc}$ in the range of 137–153 V. The increasing ε_i compensates for the fall of Γ_+ (9.0×10^{15}–8.1×10^{15} cm^{-2} s^{-1} for 0–50% O_2), so that the parameter $\varepsilon_i\Gamma_+$ keeps a near-to-constant value ($\sim 1.3 \times 10^{18}$ eV cm^{-2} s^{-} for 0–50% O_2). As such, the Ar/O_2 mixing ratio has no noticeable influence on the efficiency of the physical etching pathway. The substitution of CF_4 for O_2 at $y_{Ar} = \text{const}$ causes the slightly decreasing $-U_{dc} = 137$–125 V for 0–50%

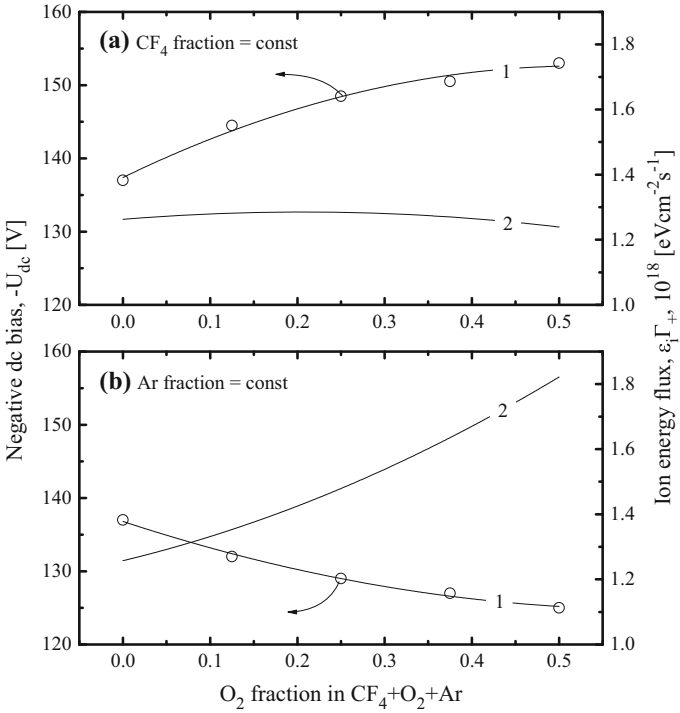

Fig. 7 Measured negative dc bias (*1*) and model-predicted ion energy flux (*2*) in $CF_4 + O_2 + Ar$ plasma: **a** as functions of O_2/Ar mixing ratio at $y_{CF_4} = \text{const}$; **b** as functions of CF_4/O_2 mixing ratio at $y_{Ar} = \text{const}$

O_2. This effect does not overcompensate an increasing tendency of Γ_+ (9.0×10^{15}–1.4×10^{16} cm^{-2} s^{-1} for 0–50% O_2), so that the parameter $\varepsilon_i\Gamma_+$ also increases in the range of 1.3×10^{18}–1.8×10^{18} eV cm^{-2} s^{-1}, or by 1.5 times. Therefore, one can obtain the intensification of the physical etching pathway in more oxygenated gas mixtures. The difference in $\varepsilon_i\Gamma_+$ between the gas systems with y_{CF_4} = const and y_{Ar} = const increases together with y_{O_2} and reaches $\sim$1.4 times at 50% O_2 (Fig. 6). However, in the points corresponding to n_F^{max} such difference appears to be less than 15%. In fact, this means the near-to-equal efficiencies of the physical etching pathways in both gas systems.

Another important thing is to compare the parameters, which determine the formation and destruction kinetics for the FC polymer film. From Fig. 7, it can be seen that the gas systems with y_{CF_4} = const and y_{Ar} = const exhibit the similar monotonic decrease in the fluxes of polymerizing radicals toward more oxygenated plasmas. Such effects are provided by the decreasing densities of both CF_2 and CF shown in Fig. 5. The main quantitative differences in Γ_{pol} appear after 40% O_2 where in the case of y_{Ar} = const this parameters falls down to zero. In the points corresponding to n_F^{max}, the flux of polymerizing radicals resulted from the variation of CF_4/O_2 mixing ratio appears to be about 7 times higher compared then that obtained by the change in Ar/O_2 mixing ratio ($\Gamma_{pol} = 8.2 \times 10^{13}$ cm^{-2} s^{-1} for 50% O_2 at y_{CF_4} = const and 6.4×10^{14} cm^{-2} s^{-1} for 25% O_2 at y_{Ar} = const). At the same time, the higher value of Γ_{pol} in the $CF_4 + O_2 + Ar$ gas system with variable CF_4/O_2 mixing ratio does not mean directly the higher polymerizing ability. Earlier, it was found that the FC polymer film growths better in the fluorine-poor plasmas. In such conditions, the polymer surface is composed by the less saturated fluorocarbon groups and thus, appears to be more reactive for the radicals coming from the bulk plasma [29, 37]. That is why the more relevant parameter for evaluation of polymerizing ability in fluorocarbon-based plasmas is the Γ_F/Γ_{pol} ratio. From Fig. 6, it can be seen that the $CF_4 + O_2 + Ar$ gas system with variable Ar/O_2 mixing ratio shows the systematically higher Γ_F/Γ_{pol} ratios in the range of 0–50% O_2 while in the points corresponding to n_F^{max} the difference between two gas systems reaches an order of magnitude (Γ_F/Γ_{pol} = 13,000 for 50% O_2 at y_{CF_4} = const and 1100 for 25% O_2 at y_{Ar} = const). Therefore, when the composition of $CF_4 + O_2 + Ar$ gas system is optimized for obtaining the highest F atom density, the variation of Ar/O_2 mixing ratio at y_{CF_4} = const simultaneously provides the much worse conditions for the deposition of the FC polymer film. However, the FC film thickness (and thus, the FC film effect on the etching kinetics) depends not only on the deposition rate, but also on the rates of FC film destruction through both etching by O atoms and physical sputtering. In our opinion, the FC film formation/destruction balance by chemical and physical pathways may be characterized by Γ_O/Γ_{pol} and Γ_+/Γ_{pol} ratios, respectively. The data of Fig. 6 allow one to conclude that an increase in O_2 fraction in a feed gas always shifts the FC film formation/destruction balance toward the destruction. Again, taking in mind the points corresponding to n_F^{max}, one can see that variation of Ar/O_2 mixing ratio at y_{CF_4} = const provides the higher Γ_O/Γ_{pol} (795 for 50% O_2 at y_{CF_4} = const vs. 111 for 25% O_2 at y_{Ar} = const) and Γ_+/Γ_{pol} (98 for 50% O_2 at y_{CF_4} = const vs. 18 for 25% O_2 at y_{Ar} = const) ratios and thus, better suppresses the polymerization. Therefore, one can definitely conclude that the $CF_4 + O_2 + Ar$ gas system with y_{CF_4} = const gives the ability to combine the higher F atom density together with lower amount of FC polymer on the etched surface. Probably, such feature may be useful for the optimization of the etching processes where the key issues are the maximum etching rate and the minimum etching residues.

Conclusion

In this work, we investigated how the changes of CF_4/O_2 (at constant fraction of Ar) and Ar/O_2 (at constant fraction of CF_4) mixing ratios in the three-component $CF_4 + O_2 + Ar$ gas mixture influence plasma parameters (electron temperature, electron and total positive ion densities, ion energy flux, densities and fluxes of neutral species) determining the dry etching kinetics. The investigation combined plasma diagnostics by Langmuir probes and zero-dimensional plasma modeling. It was shown that the variations of CF_4/O_2 and Ar/O_2 mixing ratios at constant fractions of corresponding third component have the opposite effects on T_e, n_e and n_+ due to different changes in the electron energy loss channels and formation-decay kinetics for charged species. It was found also that the substitution of CF_4 for O_2 produces the non-monotonic (with a maximum at 25% O_2) changes in both F atom density and flux. At the same time, the substitution of Ar for O_2 causes the monotonic growth of these parameters as well as provides their higher values under one and the same operating conditions. Being optimized to highest n_F, both gas systems are characterized by the quite close ion energy fluxes and thus, have no principal differences in the efficiencies of physical etching pathway. However, the variation of Ar/O_2 mixing ratio at constant fraction of CF_4 better suppresses the polymerization and thus, allows one to obtain lower amount of FC polymer on the etched surface.

Acknowledgements This work was supported by the MOTIE (Ministry of Trade, Industry and Energy) and KSRC (Korea Semiconductor Research Consortium) support program for the development of the future semiconductor device (No. 2016-10052890).

References

1. Rossnagel SM, Cuomo JJ, Westwood WD (1990) Handbook of plasma processing technology. Noyes Publications, Park Ridge
2. Rooth JR (1995) Industrial plasma engineering. IOP Publishing, Philadelphia
3. Roosmalen AJ, Baggerman JAG, Brader SJH (1991) Dry etching for VLSI. Plenum Press, New York
4. Wolf S, Tauber RN (2000) Silicon processing for the VLSI era. Process technology, vol 1. Lattice Press, New York
5. Lieberman MA, Lichtenberg AJ (1994) Principles of plasma discharges and materials processing. Wiley, New York
6. Kimura T, Ohe K (2002) J Appl Phys 92:1780
7. Rao MVVS, Sharma SP, Cruden BA, Meyyappan M (2002) Plasma Sources Sci Technol 11:69
8. Kim J-H, Chung K-H (2005) J Korean Phys Soc 47:249
9. Jenq J, Ding J, Taylor JW, Hershkowitz N (1994) Plasma Sources Sci Technol 3:154
10. Efremov AM, Kim D-P, Kim C-I (2004) Vacuum 75:133
11. Efremov AM, Kwon K-H, Shabadarova DA (2016) Izv Vyssh Uchebn Zaved Khim Khim Tekhnol 59:12
12. Kimura T, Ohe K (1999) Plasma Sources Sci Technol 8:553
13. Kimura T, Noto M (2006) J Appl Phys 100:063303
14. Plumb IC, Ryan KR (1986) Plasma Chem Plasma Proc 6:205
15. Grigoryev YuN, Gorobchuk AG (2007) Russ Microlectron 36:321
16. Kawata H, Murata K, Nagami K (1986) J Vac Sci Technol B4:6
17. Kimura T, Hanaki K (2008) Jpn J Appl Phys 47:8546
18. Chun I, Efremov A, Yeom GY, Kwon K-H (2015) Thin Solid Films 579:136
19. Efremov A, Kim JH, Kwon K-H (2014) Plasma Chem Plasma Proc 34:239
20. Son J, Efremov A, Yun SJ, Yeom GY, Kwon K-H (2014) J Nanosci Nanotechnol 14:9534
21. Johnson EO, Malter L (1950) Phys Rev 80:58
22. Sugavara M (1998) Plasma etching: fundamentals and applications. Oxford University Press, New York
23. Efremov A, Min N-K, Choi B-G, Baek K-H, Kwon K-H (2008) J Electrochem Soc 155:D777

24. Kwon K-H, Efremov A, Kim M, Min NK, Jeong J, Kim K (2010) J Electrochem Soc 157:H574
25. Li X, Ling L, Hua X, Fukasawa M, Oehrlein GS, Barela M, Anderson HM (2003) J Vac Sci Technol A 21:284
26. Gogolides E, Stathakopolous M, Boudouvis A (1994) J Phys D Appl Phys 27:1878
27. NIST Chemical Kinetica Database. http://kinetics.nist.gov/kinetics/
28. Chapman B (1980) Glow discharge processes: sputtering and plasma etching. Wiley, New York
29. Stoffels WW, Stoffels E, Tachibana K (1998) J Vac Sci Technol A 16:87
30. Christophorou LG, Olthoff JK, Rao MVVS (1996) J Phys Chem Ref Data 25:1341
31. Krishnakumar E, Srivastava SK (1992) Int J Mass Sectr Ion Proc 113:1
32. Christophorou LG, Olthoff JK (2004) Fundamental electron interactions with plasma processing gases. Springer, New-York
33. Lee C, Graves DB, Lieberman MA (1996) Plasma Chem Plasma Proc 16:99
34. Efremov AM, Kim DP, Kim CI, Trans IEEE (2004) Plasma Sci 32:1344
35. Efremov AM, Kim DP, Kim CI (2005) Thin Solid Films 474:267
36. Jin W, Vitale SA, Sawin HH (2002) J Vac Sci Technol A 20:2106
37. Kokkoris G, Gogolides E, Boudouvis AG (2000) Microelectron Eng 53:395